Structural link optimization of an echography robot

Sylvain Miossec, Laurence Nouaille

Structural link optimization of an echography robot

Sylvain Miossec* Laurence Nouaille†
PRISME Laboratory, University of Orléans, France

Abstract—
It is an interesting goal to obtain robots lighter, more precise or to minimize other criteria. Among robot optimization problems, optimizing the structure of robot links considering all its conditions of use can be a very computationally intensive problem, due to the dimension of the configuration space. Maybe for this reason, such problems has never been solved thoroughly. We considered the case of a 3-degrees-of-freedom echography robot. We optimize the shape of two links to minimize the weight and deformation under an end-effector force condition, and whatever the robot configuration. In order to obtain a rapid optimization, we use a non-uniform beam model for links with sensitivity computations. We proposed an easy-to-solve compromise formulation between two criteria. We showed that some substantial weight decrease could be obtained while keeping small deformations, with reasonable computation times, and that several configurations must be considered simultaneously.

I. Introduction

Design optimization of robots is challenging to obtain more precise, lighter, faster, less energy-consuming or stronger robots. To obtain this goal, it is possible to choose the robot structure (number, type and position of joints) the links shape, the choice and position of the actuators. In this paper we are interested in the optimal choice of links shape. Our contributions on this problem are:

- to optimize the robot shape under a strength constraint of its structure. At first, this problem is not different from structural optimization made in civil engineering or engineering design. Our contribution is to consider the complexity of robot due to its various configurations, and to environment forces it may undergo. This general problem is presented section II.
- to approximate the problem, compute its gradients and use a gradient-based optimization method to obtain a fast and robust optimization, see section III.
- to propose a compromise formulation between two criteria that can be easily and efficiently solved.
- to apply this method to a 3-degrees-of-freedom echography robot section IV to analyze the optimal solution, and to demonstrate the weight improvement obtained with the proposed approach section V.

*E-mail: sylvain.miossec@bourges.univ-orleans.fr
†E-mail: laurence.nouaille@bourges.univ-orleans.fr

Our approach is finally compared to previous works in section V-E.

II. The problem of static structural optimization of a robot

We consider the design of robots whose kinematic structure has already been chosen in a previous design stage under geometric and kinematic requirements. In this study, we are interested in the choice of the links shape parameters, such as thickness, beam section dimensions, and any other geometric parameters independent of the joints relative position. All shape parameters of links are grouped in the vector $p \in \mathbb{R}^{n_p}$. We consider the set of external load forces $F \in \mathcal{F} \subset \mathbb{R}^{n_f}$. n_f could be more than 6 if forces apply not only on a single point. We also consider the joint variables q in the configuration space $\mathbb{R}^{n_q}$. The robot static equations enable the writing of the 6-component joint forces and torques vector of link i F_i with respect to joint angles q and external loads F.

$$F_i = J(q)F \; \forall i = 1..n_q \tag{1}$$

where $J(q)$ is a Jacobian matrix.

We must consider a static structural model of links to get end-effector displacement and internal stress tensor $\boldsymbol{\sigma}$. For each link this tensor depends on forces applied on this body and the point P of the link.

$$\boldsymbol{\sigma_i}(p, P, F_i, F_{i-1}) \forall P \in \text{link i} \tag{2}$$

For notation simplicity, we only consider serial robots submitted to joint forces with previous and next body. But this notation can be extended to tree-like and parallel robots. We do not consider any stiffness for motors. In a static case, it could be infinite with an integral term in the joint control law. Any other source of joint deformation could be taken into account in a 3D structural model.

In this paper, we address the problem of optimally choosing the shape parameters p to minimize a criterion $C(p)$ of the robot for the whole configuration space and external load space under a yield criterion and additional constraints $g(p, q, F) < 0$. The mathematical formulation of this de-

sign optimization problem is the following.

$$\min_{p\in\mathbb{R}^{n_p}} C(p)$$
subject to
$$\begin{array}{l}\sigma_{\text{VM}\,i}(p,P,F_i,F_{i-1}) < \sigma_y \\ F_i = J(q)F \\ g(p,q,F) < 0\end{array} \quad \left\{\begin{array}{l}\forall P \in \text{link i} \\ \forall i \in [1,n_q] \\ \forall q \in \mathbb{R}^{n_q} \\ \forall F \in \mathcal{F}\end{array}\right. \tag{3}$$

Where σ_{VM} is the Von Mises stress computed from $\boldsymbol{\sigma}$ that must be inferior to the yield strength σ_y in order to avoid yield. This problem is a high-dimensional semi-infinite nonlinear optimization problem, see [1]. Semi-infinite optimization problems carry an infinite number of constraints, which is the case of constraints on Von Mises stress that take place whatever the point P, robot configuration q and external load forces F. In this case, the semi-infinite space is of dimension $n_q + n_f + 3$ (the 3-dimensional space being the space of position of yield constraint). We will see in the next section how this problem is approximated in order to solve it numerically.

III. Approximation of the problem for numerical solving

A. Structural model of the robot

For the structural model, any Finite Element algorithm could be used, but as a first step, we choose the simplest beam model. This model is adapted for robot elongated links. For improved solution, we consider non-uniform links by discretizing them in piece-wise uniform beams. We also neglect the links gravity forces compared to the end-effector force and motors weight. For the computation of the internal stress, we considered bending, compression, torsion, as well as shear forces and moments. The beams section parameters will constitute the shape parameters of such a structural model.

B. Discretized optimization problem

In order to solve the problem (3) with nonlinear optimization methods, the semi-infinite constraints are discretized. We will note $\mathbb{P}_i \in$ link i the set of discretized geometric points belonging to link i, $\mathbb{Q} \in \mathbb{R}^{n_q}$ the set of discretized configuration points belonging to configuration-space, $\mathbb{F} \in \mathcal{F}$ the set of discretized external loads. The new discretized optimization problem is then,

$$\min_{p\in\mathbb{R}^{n_p}} C(p)$$
subject to
$$\begin{array}{l}\sigma_{\text{VM}\,i}(p,P,F_i,F_{i-1}) < \sigma_y \\ F_i = J(q)F \\ g(p,q,F) < 0\end{array} \quad \left\{\begin{array}{l}\forall P \in \mathbb{P} \\ \forall i \in [1,n_q] \\ \forall q \in \mathbb{Q} \\ \forall F \in \mathbb{F}\end{array}\right. \tag{4}$$

It is important to notice that the evaluation of all constraints will need n_c FEM computations, where $n_c = n_{fd} \times n_{qd}$ with n_{fd} the number of discretized external loads and n_{qd} the number of discretized configuration points (in the hypothesis that all discretized loads apply to all discretized configuration). In the case where $\mathcal{F}$ would depend on q, computation would be different.

C. Gradients computation

To improve the convergence speed and robustness, we computed the gradients of the criteria and the constraints. To this end, we used the open-source OpenSees finite element software [2], developed for the seismic response of structural and geotechnical systems. OpenSees includes sensitivity computations, as well as the parameters management, which allows us to compute the exact internal stress gradients, constraints and criteria.

D. Optimization method

We used the sequentially quadratic programming (SQP) method NPSOL [3]. This is a gradient-based method that will find very efficiently a local solution.

IV. Application to Estele echography robot

A. Estele robot presentation

This work takes place in the context of tele-echography, which consists in a specialist controlling at a distance the motion of an ultra-sound probe through an echography robot. The analysis of echographic exams [4] showed two steps: a search for the organ to observe, and then the observation of the organ itself Fig. 1(a). For the complete exam 6 degrees of freedom are necessary. But for an emergency situation a portable robot is more adapted. It has been showed 6 dof robots are too heavy to be portable, therefore portable robots are usually restricted to 4 dof: 3 rotational dof, and one translation normal to the contact. Such dof are adapted to the second step of organ observation. Missing dof are provided by the person holding the robot that can be asked to change the position of the robot on the patient. The gesture analysis additionally showed that expert is observing essentially around the normal to the patient Fig. 1(b). Robots are then better adapted if the center of their workspace is around this normal.

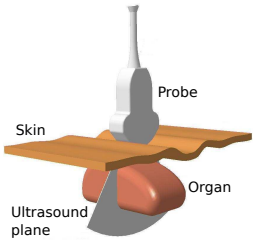

(a)Echography exam

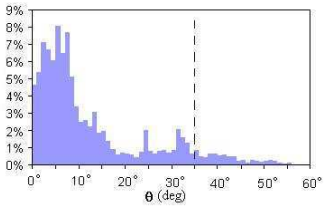

(b)Time repartition of probe orientation with respect to normal of contact

Fig. 1. Analysis of echographic exams.

(a)Photo

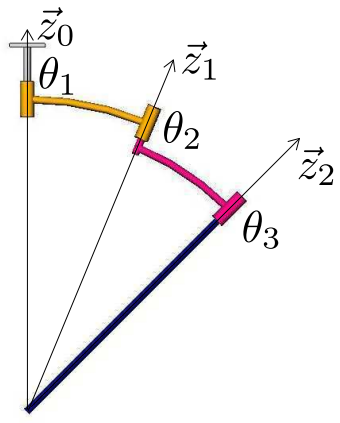

(b)Kinematic diagram

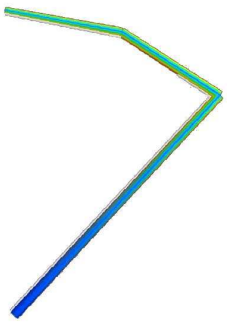

(c)Structure in same configuration

Fig. 2. Estele prototype.

The work of this paper is applied to the Estele echography robot presented Fig. 2 [5]. This is a serial spherical wrist robot composed of three revolute joints (θ_1, θ_2, θ_3) with concurrent axes, which gives a remote center of motion, see Fig. 2(b). An additional fourth prismatic joint is also present to control the contact force applied, but will not be considered in this paper. For the Estele robot, the angle between joint axes is of $22.5°$ so that the workspace is a cone of $45°$ with the vertical. The distance between the center of rotation and the last revolute joint center is 18cm in order for the echographic probe to fit with its cable.

B. Optimization problem

B.1 Parameters

The presented kinematic dimensions are taken for granted in this study, and we will focus on the shape optimization of the two first bodies of the robot. As said previously those bodies are modeled by non-uniform beams approximated by piece-wise uniform beams. We considered all beams as tubes defined by inner radius R_0 and outer radius R_1. We had to implement the computation of internal stress in a beam section, that does not exist in the OpenSees software. For a tube, we computed analytically the expression of stress due to compression, bending, torsion and shear. We considered N_b beams for first and second links, and only one beam for the third. This makes a total of $2 \times N_b + 1$ parameters in p.

B.2 Loads and configurations

The load requirement for the robot is to sustain a maximum vertical force of 20N on the probe. We considered also the weight of motors on the joints: 277g for the second joint, 394g for the third joint (including the fourth prismatic joint), as well as the weight of the probe of 100g. We also considered the situation where no contact force is applied on the probe, which correspond to a situation of the robot moved by the technician in free space.

First and last joints θ_1 and θ_3 have no effect on the forces applied on first and second links. Except for the third link that will undergo the same load in all directions for all third angle values θ_3; but since this link is a shape of revolution, the θ_3 orientation has no effect on the optimal tube parameters. Configuration space that must be considered for this study is then only the space of second joint θ_2. Due to a symmetry, we consider only values between $0°$ and $180°$.

B.3 Criteria

The problem considered is a compromise between two contradictory criteria: the mass of the robot $M(p)$, and the deformation of the robot end-effector subject to the forces applied $d(p, q, F)$ that can be seen as the precision we can obtain for the end-effector. The mass $M(p)$ includes both the structure mass, the motors mass 671g, and an approximate probe mass 100g. At first we dealt with the compromise between both criteria by minimizing $M(p)$ under a maximum acceptable displacement on $d(p, q, F)$. Since criteria are contradictory, solution is at specified acceptable displacement or limited by other constraints. As will be seen on the Pareto frontier Fig. 3 structure mass is then very light and displacement important, and it is possible to decrease greatly the displacement with relatively small increase in mass $M(p)$. This lead us to choose another point on the Pareto frontier: the point from which a relative decrease of one criteria gives the same relative increase of the other criteria. We show in ANNEXE that we can find this point by minimizing criteria $C(p) = ln(M(p)) + ln(\max_{q,F} d(p, q, F))$, which can be reformulated in

$$\begin{aligned} &\min_{p,s} C(p, s) = ln(M(p)) + ln(s) \\ &\text{subject to} \\ &d(p, q, F) - s < 0 \quad \begin{cases} \forall q \in \mathbb{Q} \\ \forall F \in \mathbb{F} \end{cases} \end{aligned} \tag{5}$$

where s is a slack variable that will equal the maximum displacement among configurations and loads at the solution. Additional constraints on the maximum values of both criteria had to be provided, since, as we will see, solution of proposed compromise can be for an infinite value of a criterion. 3cm was chosen for the displacement, and 10% of the mass of motors and probe for structure mass, corresponding to 77.1g.

B.4 Constraints

The yield constraints on the Von Mises stress σ_{VM} are considered on the discretized volume of the beams. We considered a grid of 16 pieces on the circumference, one point per beam along the axis of the beam. For our problem, we also noticed that the maximum of the constraints were on the exterior surface. To keep the problem as light as possible, we added progressively the points that had Von Mises stress greater than the yield strength σ_y.

We also added some constraints to problem (4) in order to obtain a minimum thickness of the tubes and a maximum radius of the tubes. Otherwise with the defined problem, we obtain solutions with too thin and large tubes, as will be detailed later.

We considered two materials for the robot: aluminum (Young modulus $E = 69GPa$, Poisson's ration $\nu = 0.33$, yield strength $\sigma_y = 100MPa$) and polyoxymethylene (POM, Young modulus $E = 3GPa$, Poisson's ration $\nu = 0.35$, yield strength $\sigma_y = 50MPa$).

V. Results

Optimizations were performed for 8 configurations with θ_2 varying from 0° to 157.5° for each of the two load conditions. We considered $N_b = 10$ beams for first and second link. Aluminum optimizations were performed for tubes of minimal thickness 1mm and maximal radius of 15mm. POM optimizations were performed for tubes with a minimal thickness of 1.5mm and maximal radius of 15mm.

A. Pareto frontier of mass and displacement criteria

Pareto frontier Fig. 3 was obtained by performing several mass minimization problems with varying maximum constraint on displacement.

B. Case of minimum mass

For aluminum, convergence was obtained in 34 iterations and 3min, as can be seen Table I. The optimal shape of bodies obtained is presented Fig. 4. External radius range approximately from 2mm to 3mm, with a thickness of 1mm everywhere. Characteristics of the solution are presented Table I. The solution obtained is at the extremity of the aluminum Pareto of Fig. 3. Von Mises stress for all considered configurations/loads of the optimal structure are presented Fig. 5, and Fig. 6 focus on the zones of maximum stress that are at the limit of yield.

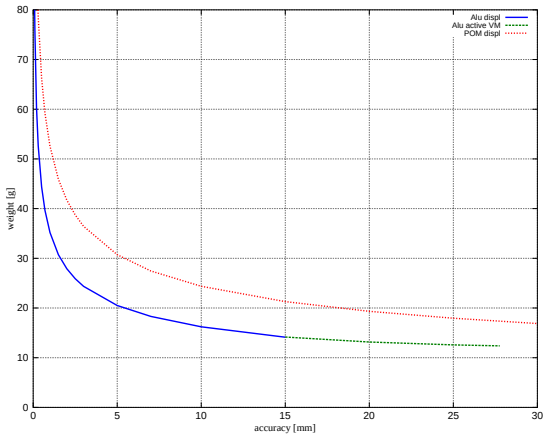

Fig. 3. Pareto frontier of structure mass with respect to displacement for aluminum and POM. The aluminum curve is the one below, aluminum allowing lighter structure for a same displacement. The aluminum Pareto between 15mm and 27.8mm correspond to a solution with active yield constraints. The curve end at 27.8mm since it is not possible to obtain lighter structure satisfying yield constraints (in the space of non-uniform tubes considered).

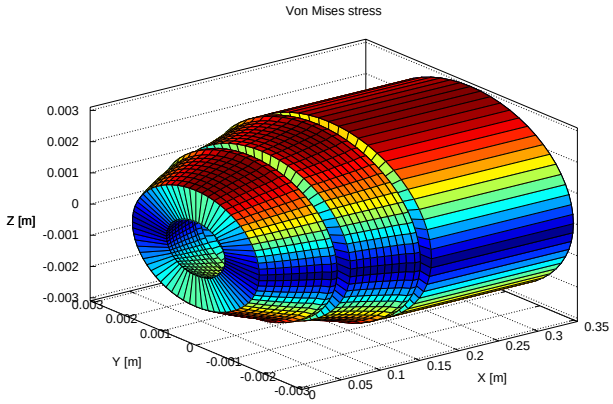

Fig. 4. Minimum mass shape of aluminum bodies with Von Mises Stress represented for $\theta_2 = 0$. First link is on the left, second in the middle, third on the right.

For POM, we obtained a solution of weight 11.3g but a norm of displacement of the end-effector of 25cm, which is even larger than the size of the links. The corresponding solution is outside of the POM Pareto of Fig. 3. Our beam model is not valid anymore, and this is much too important for our application. This echography robot is used in a visual feedback loop including a human that can compensate for robot deformations, but not to that point. We then added a previously unformulated requirement as a maximum displacement of end-effector by 3cm. The solution obtained is at the extremity of the POM Pareto representation Fig. 3. Convergence characteristics and optimal solution are presented Table I. External radius ranges from 5mm to 7mm,

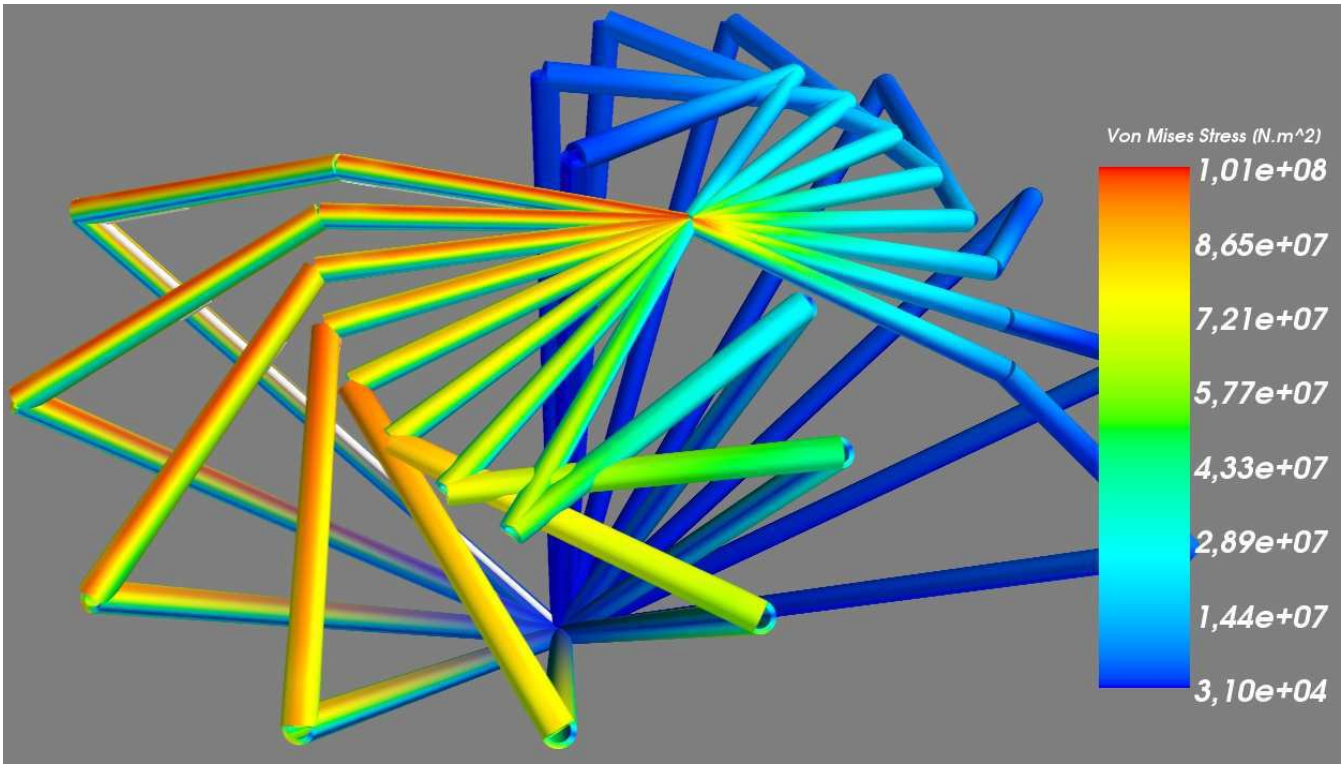

Fig. 5. Von Mises stress for minimum mass aluminum structure for all configurations considered. The 8 configurations on the left correspond to the case of a vertical force of 20N on the end-effector. The 8 configurations on the right correspond to the case of no end-effector force, that is, only submitted to its own weight.

with a thickness of 1.5mm.

TABLE I. Results of structure mass minimization, with aluminum or POM, for one configuration or 8 configurations.

	Config.	Iter.	Time	Weight	$\sigma_{VM\ max}$	Disp. max
Alu.	8	34	3min	12.847g	101MPa	2.78cm
	$\theta_2 = 0°$	41	30s	12.835g	106MPa	2.79cm
	$\theta_2 = 90°$	23	16s	11.117g	117MPa	2.69cm
POM	8	177	34min	21.935g	17.8MPa	3cm
	$\theta_2 = 0°$	86	1min30s	21.935g	17.48MPa	3cm
	$\theta_2 = 90°$	374	11min	21.228g	19.7MPa	3.31cm

We performed the same optimization as previously, but for the restriction that only the straight arm configuration $\theta_2 = 0°$ was considered for constraints, as well as for only the configuration $\theta_2 = 90°$. All the convergence and solution data are presented Table I.

C. Compromise case

This problem corresponds to (5) with additional maximum structure mass of 77.1g and maximum acceptable displacement of 3cm. The solutions obtained are at the maximum structure mass of 77.1g, see Table II. Von Mises constraints were not included in the optimization process since they are not active at the solution. They were slowing down the computations and preventing the optimization algorithm to converge properly for numerical reasons. To solve it properly, Von Mises constraints could be added progressively during optimization process when they become violated. The aluminum optimal solution is composed of tubes of thickness 1mm, and radius from 13.5 to 15mm. The POM optimal solution is composed of tubes of radius 15mm, and thickness from 1.5mm to 3mm.

TABLE II. Results of structure mass-displacement compromise, with aluminum or POM.

	Config.	Iter.	Time	Weight	$\sigma_{VM\ max}$	Disp. max
Alu.	8	109	41s	77.1g	2.96MPa	0.1mm
POM	8	232	1min 11s	77.1g	1.78MPa	1.2mm

D. Discussion

D.1 Characteristics of solutions

In all cases, the solution was at the minimum thickness (1mm for aluminum and 1.5mm for POM) or at the maximum tube radius. If such constraints were not considered, the optimal solution would be for a null thickness with an infinite radius. To prevent this, the real physical constraint that should be added is the local buckling avoidance. But such constraint is difficult to express. And the limit of thickness could also be considered as a manufacturing constraint, since too thin bodies are difficult to produce. Maximum radius constraint can be considered as a limit on

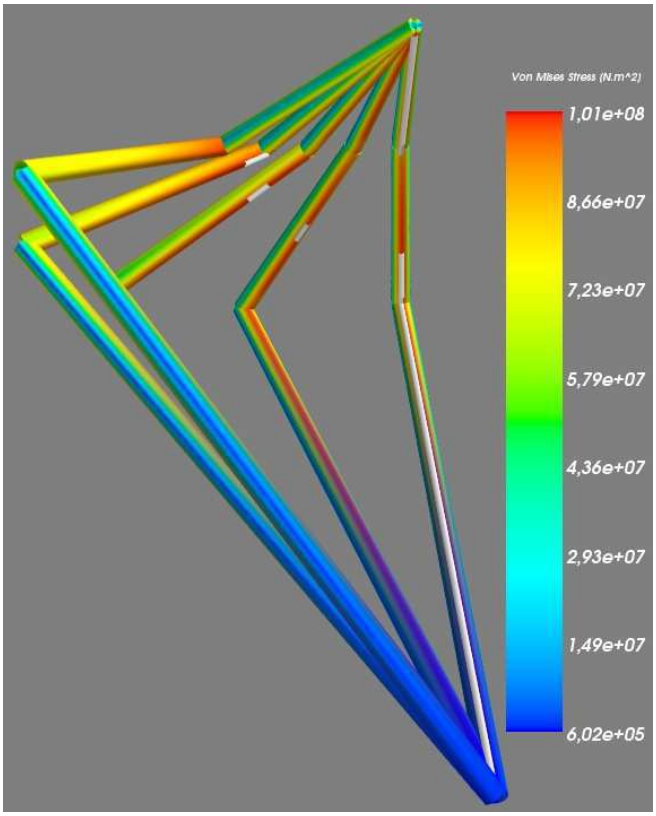

Fig. 6. Von Mises stress for minimum mass aluminum structure optimized for all configurations considered. Maximum stress of a section is highlighted with white lines. Only configurations with maximum stress are represented.

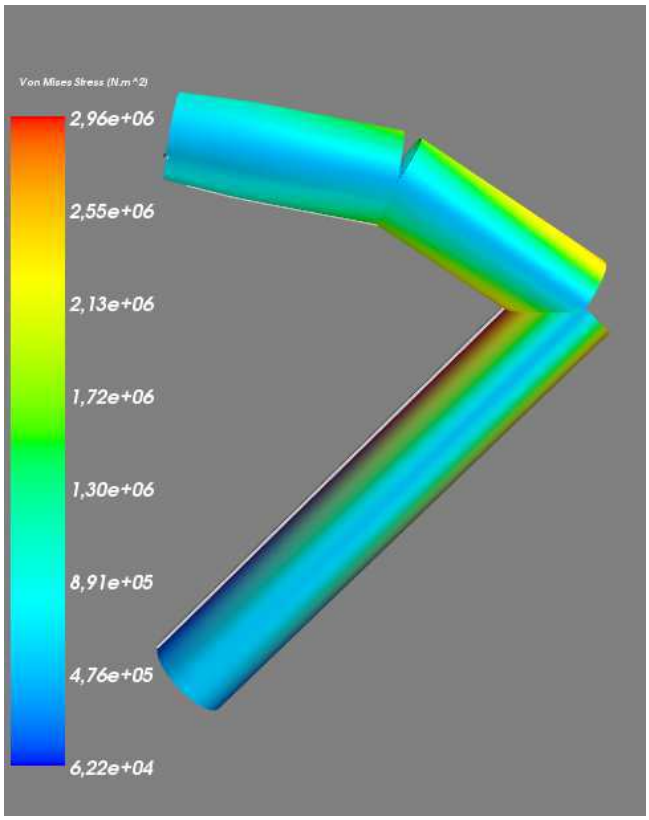

Fig. 7. Aluminum structure optimized with compromise criterion.

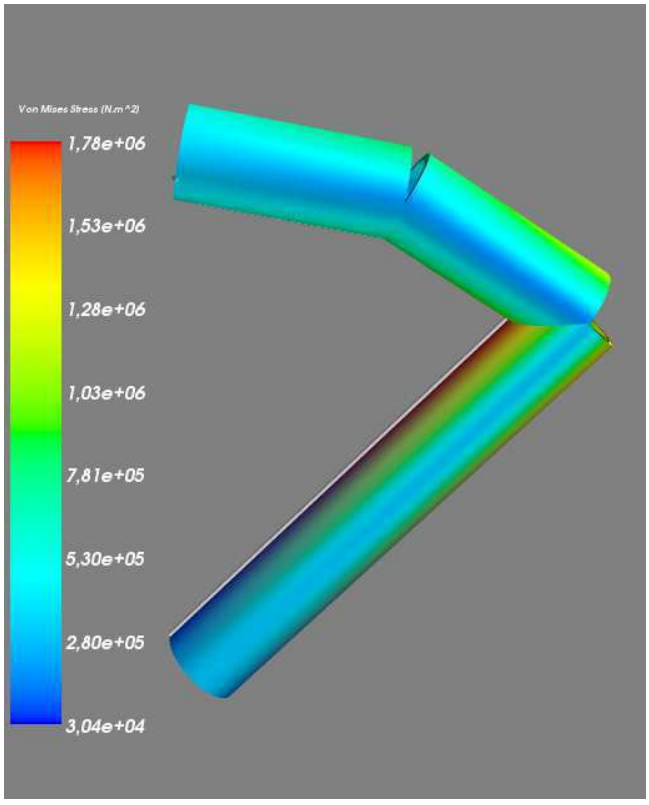

Fig. 8. POM structure optimized with compromise criterion.

bulkiness of the links.

Minimum mass solutions are at the right extremities of Pareto frontier Fig. 3. What can be additionally observed is that displacement can be decreased a lot, while the structure mass is increased only slightly relatively to the total mass including motors and probe. It is therefore not interesting to stick to the minimum mass solution. That's why we translated this compromise in choosing the Pareto point with opposite relative variations of both criteria. Practically, if one move locally from this point along the Pareto frontier, when a criterion increase for example of 10%, the other criterion decrease also of 10%. We discuss this compromise later on.

For the case of minimum mass and several configurations, the other active constraints at the optimal solution depends on material: for aluminum structure those are the yield constraints ; for POM structure the only other active constraint is the displacement limitation. When yield constraints are active, they are active for each section only one time in the configuration space, as can be seen on Fig. 6. Such a solution seems to present a decoupling between all sections. Knowing this characteristic of the optimal solution, a dedicated algorithm could be developed to obtain the solution in a much faster computation.

We obtained that the use of aluminum gives a lighter or

more rigid robot than POM for all problems. The convergence is fast when limiting constraints are the yield condition on the Von Mises stress. However convergence is slow when the limiting constraint is the displacement limit while Von Mises stress constraints are still defined in the problem. Removing those non-active Von Mises stress constraints improved convergence (which theoretically should not be the case). It then seems all non-active yield constraints give numerical problems to the optimization program. In Table I we observe a slight yield constraint violation for the minimum mass aluminum structure with 8 configurations. It is due to the fact the discretization of the Von Mises stress is tighter for the presentation of the solution than during the optimization. This could be solve by adding the constraints that are not satisfied in a new optimization problem that we solve again.

For the compromise solution, it can be observed solutions are at the maximum allowed structure mass. This can be explained by analyzing roughly the dependence of criteria with respect to radius of tubes in bending (which is the main deformation taking place in the robot). For thin-walled tubes of radius R and thickness e, in first approximation the mass is homogeneous to Re, and the displacement is homogeneous to $\frac{1}{R^3 e}$. Minimizing (5) is in first approximation equivalent to minimize $-2\ln(R)$ which gives a Radius R tending to infinity and a displacement tending to 0 on Pareto frontier. It explains why we obtain the minimum displacement allowed by the maximum mass constraint.

Analyzing the compromise solution, with tubes of slight radius or thickness change, one could rather consider using uniform tubes instead, which would decrease slightly performance of the solution, but would be much easier to manufacture.

D.2 Interest of the approach

The Pareto frontier Fig. 3 gives insight in the problem, but require many optimizations. For more complex robot designs or problems with more criteria, it could be very time consuming to obtain. In such a context, the compromise optimization formulation proposed in this paper could be very interesting.

For the case of the minimum mass aluminum structure that is constrained by yield, the solution satisfying the constraints of 8 configurations is only slightly better than the solution satisfying only constraints of configuration with $\theta_2 = 0^\circ$ (weight is almost similar, the yield constraint violation is of about 5%). In this case, optimizing only one configuration could be enough. However it was the best configuration we could choose. For the configuration $\theta_2 = 90^\circ$ (which include a point of maximal stress for a section, see Fig. 6) solution obtained is not as optimal: the weight is decreased but at the expense of the yield constraint violation of about 16%. And for a random configuration, it could be even worse. For other cases structure is constrained by displacement of end-effector due to the load, and only one constraint is active. So taking the configuration with $\theta_2 = 0^\circ$ that gives the maximum displacement, the exact solution can be obtained. For example, considering only the configuration with $\theta_2 = 90^\circ$ gives a violation of the constraint of about 10% for the mass minimization of POM structure.

Minimum mass solution presented is not a good compromise. However this solution shows the interest in some cases of taking into account several configurations. We could imagine other problems where taking several constraints are important: if weight is much more important than precision, if load and configuration space are complicate we could have several maximum displacement loads/configurations.

We also compare our results with the original Estele echography robot. The equivalent structure parts of the Estele robot account for a weight of 740g in POM, while we found minimum weight of 22g in POM and 13g in aluminum, and 77.1g for our mass-displacement compromise. This is a very large difference that can be explained primarily by the fact Estele echography robot was not optimized. Another explanation why we found a very light structure is because of the simplifications we considered. We will present them in the next section.

D.3 Limitations of the approach

The beam model we choose does not allow to represent/choose the shapes near joints, that are complicate because of the integration of the joint, cables, motors, ... Furthermore, the beam model is only valid far from the extremities of the links. The current study then gives only an optimal choice valid near the center of each link. We also neglected gravity forces of links. The difficulty to integrate gravity forces of links is that it depends on the shape of the structure. Taking into account them will complicate the problem since loads on beams will depend on shape parameters.

Not making most of previous approximations will probably produce an heavier/less precise robot. However some improvement could still give some weight/precision gain: to consider different sections shape (in particular for the first link that is essentially submitted to bending, the optimal shape is an I section) and to include a precise non-buckling constraint in addition to the thickness constraint. The buckling is a global characteristic of a link, that can not be reduced to each beam of the piece-wise representation. Furthermore, observing local buckling of tube walls require 3D FEM model. Hence some problem to integrate buckling with the FE software beam model.

E. Related work

Many works have been devoted to the optimization of structures, see for example the review paper [6], and the books [7], [8], [9]. But they usually consist in non-reconfigurable structure (like robots) and single loaded

studies. However, [7] was very interesting: it gives analytical solutions of optimal beams, taking into account both buckling and yield constraints. It gave insight on the optimal section shape, depending on the type of loads. However the results and approaches presented were not reusable for non-uniform beams submitted to all type of constraints. We then had to use numerical methods. [9] identified three types of numerical shape optimization methods:

- the parametric method which consists in choosing some basic geometric parameters from which the shape is defined. This method is adapted for the optimization of parametrized mechanical designs performed with CAD software.
- the geometric method, which consists in considering the shape model as the FE mesh, that allows to parametrize the shape more precisely, but does not solve the problem of topology choice.
- the topology method, which consists in discretising the space and determining where to put some material. It addresses the problem of topology choice.

The approach presented in this paper is a parametric one.

Surprisingly, in the robotic field, few works have been devoted to the structural optimization of robots, maybe because it is a very high-dimensional, difficult to solve problem. Many design optimization studies of robots are limited to kinematic properties, see [16], [17], [18], [19]. The few studies that we found to consider structural aspects are [10], [11], [12], [13], [14], [15]. Comparison of these works with this paper is presented in Table III. It can be seen that most structural optimization of robots, are interested into stiffness and displacement of the end-effector or vibrations. Only the work of [10] was also interested in strength of the robot. It computed the maximal forces in the worse configuration, and optimized the robot only for this configuration/load. However, we have seen in this paper Fig. 6 that the maximum stress can take place on several configurations, and that several configurations must than be taken into account simultaneously. Another contribution that we did not found in those papers is the computation of gradients to increase robustness and speed of convergence. We obtained reasonable times in Table I. On the contrary, in [13], they obtained optimization times of several days and weeks. Even if they optimized a more complex problem of a 9-links parallel robot modeled with 3D FE elements on a trajectory, we hope our approach with gradients computation would allow for faster computation.

VI. Conclusions and future works

A. Conclusions

We presented the general problem of shape optimization of robots, and a simple method to obtain a problem that can be solved with non-linear optimization algorithms. We used beam structural model that can be applied to optimize the shape of robots composed of elongated bodies approximated with piece-wise uniform beam. The use of OpenSees FE software allows for gradient computation for efficient and robust optimization. It also allows to program easily the optimization of new problems using a scripting language. We analyzed the problem and proposed a an easy-to-solve formulation that gives a good compromise between two criteria. We also obtained interesting results that show the need for optimization in the whole configuration-space. We finally showed that the approach can decrease dramatically the weight of the structure. However the method must still be assessed and developed in order to be more realistic and to be usable more widely.

B. Future Works

In the near future, we will consider other section shapes, investigate the inclusion of buckling constraints for non-uniform beams, and finally consider more general and realistic 3D structural models. We will also inverstigate if our compromise formulation can be extended for more than 2 criteria optimization problems. On a longer term, we will investigate the use of geometric and/or topology optimization methods, and consider dynamic robot model and vibration model.

ANNEXE: Demonstration of problem to solve to obtain the point on Pareto frontier that satisfy opposite relative variations of two criteria

Let's consider the Pareto frontier of problem with two criteria $C_1(x) > 0$ and $C_2(x) > 0$ to minimize in function of variables x. A point of this Pareto frontier for $C_1(x) = \alpha$ can be obtained by solving the following problem:

$$\begin{array}{l} \min\limits_{x} C_2(x) \\ \text{s.t. } C_1(x) < \alpha \end{array} \tag{6}$$

Let's note $x_{opt}(\alpha)$ the optimal parameter x obtained by solving (6). The Pareto frontier equation can then be written $C_2(x_{opt}(\alpha))$. The desired point on Pareto frontier with opposite relative variations is given by $\frac{dC_1}{C_1} = -\frac{dC_2}{C_2}$. With previous definition of Pareto frontier, we obtain

$$\frac{\partial C_2(x_{opt}(\alpha))}{\partial \alpha} = -\frac{C_2(x_{opt}(\alpha))}{\alpha} \tag{7}$$

We will show that the problem:

$$\min_x ln(C_1(x)) + ln(C_2(x)) \tag{8}$$

is giving as a solution the point of the Pareto frontier that satisfy (7). For this, we should first notice that this problem will give us a solution on the Pareto frontier: by reductio ad absurdum, if optimal solution of (8) was not on Pareto frontier we would be able to decrease both criteria, which would mean we could decrease more the criterion of (8). Then, let's consider the optimality condition of problem (8):

$$\frac{1}{C_1}\frac{\partial C_1}{\partial x} + \frac{1}{C_2}\frac{\partial C_2}{\partial x} = 0 \tag{9}$$

TABLE III. Comparison of studies on structural optimization of robots. A static robot model with a dynamic FE model means FE dynamic computations are valid only for small displacements. A trajectory for the Configuration/Load means that some Criteria/Constraints are defined on a trajectory. The crosses "X" for the Criteria/Constraints indicate which type of Criteria/Constraints were considered. SQP stands for the Sequential Quadratic Programming optimization algorithm, and GA for the Genetic Algorithm.

		This paper	[10]	[11]	[12]	[13]	[14]	[15]
FE model	type	static	static	dynamic	static	dynamic	dynamic	dynamic
	size	1D	3D	1D	1D	3D	1D	1D
Robot model		static	static	dynamic	dynamic	dynamic	static	dynamic
Config.×Load space		8×2	max×1	traj.	traj.	traj.	10×2	traj.
Shape		non-uniform	non-uniform	non-uniform	non-uniform	uniform	uniform	non-uniform
Crit./Constr.	displ.			X	X	X		X
	vibration freq.			X			X	
	stress	X	X					
	weight	X	X	X	X			
Optimization		SQP	Pro/Mechanica	SQP	GA	SQP	by hand	GA

Solution of (8) being on Pareto frontier, we can perform a scalar product of optimality condition (9) with $\frac{\partial x_{opt}(\alpha)}{\partial \alpha}$,

$$\frac{1}{C_1}\frac{\partial C_1}{\partial x}^T \frac{\partial x_{opt}(\alpha)}{\partial \alpha} + \frac{1}{C_2}\frac{\partial C_2}{\partial x}^T \frac{\partial x_{opt}(\alpha)}{\partial \alpha} = 0 \quad (10)$$

where $\alpha = C_1(x_{opt}(\alpha))$. By deriving $C_1(x_{opt}(\alpha))$ and $C_2(x_{opt}(\alpha))$ with respect to α we obtain

$$\begin{aligned} \frac{\partial C_1(x_{opt}(\alpha))}{\partial \alpha} &= \frac{\partial C_1}{\partial x}^T \frac{\partial x_{opt}(\alpha)}{\partial \alpha} = 1 \\ \frac{\partial C_2(x_{opt}(\alpha))}{\partial \alpha} &= \frac{\partial C_2}{\partial x}^T \frac{\partial x_{opt}(\alpha)}{\partial \alpha} \end{aligned} \quad (11)$$

Finally replacing those last expressions in (10) gives us the condition of opposite variations of the criteria (7).

References

[1] R. Hettich and K. Kortanek, "Semi-infinite programming: Theory, methods, and application," *SIAM review*, vol. 35, no. 3, pp. 380–429, 1993.

[2] S. Mazzoni, F. McKenna, M. H. Scott, and G. L. Fenves, *The OpenSees Command Language Manual*, Pacific Earthquake Engineering Center, Univ. of Calif., Berkeley, 2007. [Online]. Available: http://opensees.berkeley.edu

[3] P. E. Gill, W. Murray, M. A. Saunders, and M. H. Wright, *User's guide for NPSOL 5.0*.

[4] L. Al Bassit, "Structures mécaniques à modules sphériques optimisées pour un robot médical de télé-échographie mobile," Ph.D. dissertation, Université dOrléans, 2005.

[5] C. Delgorge, F. Courrèges, L. Al Bassit, C. Novales, C. Rosenberger, N. Smith-Guerin, C. Brù, R. Gilabert, M. Vannoni, G. Poisson, and P. Vieyres, "A tele-operated mobile ultrasound scanner using a light weight robot," *IEEE Transactions on Innovation Technology in Biomedicine*, vol. 9, no. 1, pp. 50–58, Mars 2005.

[6] J. Arora and Q. Wang, "Review of formulations for structural and mechanical system optimization," *Structural and Multidisciplinary Optimization*, vol. 30, pp. 251–272, 2005.

[7] D. W. Rees, *Mechanics of Optimal Structural Design*. Wiley, 2009.

[8] J. S. Arora, Ed., *Optimization of Structural and Mechanical Systems*. World Scientific, 2007.

[9] G. Allaire, *Conception optimale de structures*. Springer, 2007, in french.

[10] F. Bidault, C.-P. Teng, and J. Angeles, "Structural optimization of a spherical parallel manipulator using a two-level approach," in *Proceedings of DETC'01*, 2001.

[11] U. S. Dixit, R. Kumar, and S. K. Dwivedy, "Shape optimization of flexible robotic manipulators," *Journal of Mechanical Design*, vol. 128, pp. 559–565, 2006.

[12] C. Leger, "Automated synthesis and optimization of robot configurations: an evolutionary approach," Ph.D. dissertation, 1999.

[13] R. Neugebauer, W.-G. Drossel, C. Harzbecker, S. Ihlenfeldt, and S. Hensel, "Method for the optimization of kinematic and dynamic properties of parallel kinematic machines," in *Annals of the CIRP*, 2006.

[14] J. Roy and L. L. Whitcomb, "Structural design optimization and comparative analysis of a new high-performance robot arm via finite element analysis," in *Proceedings of the 1997 IEEE International Conference on Robotics and Automation*, 1997.

[15] Y. Zhu, J. Qiu, and J. Tani, "Simultaneous optimization of a two-link flexible robot arm," *Journal of Robotic Systems*, vol. 18, no. 1, pp. 29–38, 2001.

[16] F. Chapelle and P. Bidaud, "Evaluation functions synthesis for optimal design of hyper-redundant robotic systems," *Mechanism and Machine Theory*, vol. 41, pp. 1196–1212, 2006.

[17] L. Nouaille, "Démarche de conception de robots médicaux - application à un robot de télé-échographie," Ph.D. dissertation, 2009.

[18] E. Bouyer, S. Caro, D. Chablat, and J. Angeles, "The multiobjective optimization of a prismatic drive," in *Proceedings of DETC'2007*, 2007.

[19] J.-P. Merlet, "Optimal design of robots," in *Robotics: Science and systems*, Boston, June 2005. [Online]. Available: http://hal.archives-ouvertes.fr/inria-00000473/en/